

The structure of ^{16}C : Testing shell model and *ab initio* approaches

M. Petri,^{1,2,*} S. Paschalis,^{1,2} R. M. Clark,¹ P. Fallon,¹ A. O. Macchiavelli,¹ K. Starosta,^{3,4,5} T. Baugher,^{4,5} D. Bazin,⁴ L. Cartegni,⁶ H. L. Crawford,^{4,7} M. Cromaz,¹ U. Datta Pramanik,⁸ G. de Angelis,⁹ A. Dewald,¹⁰ A. Gade,^{4,5} G. F. Grinyer,⁴ S. Gros,¹ M. Hackstein,¹⁰ H. B. Jeppesen,¹ I. Y. Lee,¹ S. McDaniel,^{4,5} D. Miller,^{4,5} M. M. Rajabali,⁶ A. Ratkiewicz,^{4,5} W. Rother,¹⁰ P. Voss,^{4,5} K. A. Walsh,^{4,5} D. Weisshaar,⁴ M. Wiedeking,^{11,12} B. A. Brown,⁵ C. Forssén,¹³ P. Navrátil,¹⁴ and R. Roth²

¹*Nuclear Science Division, Lawrence Berkeley National Laboratory, Berkeley, California 94720, USA*

²*Institut für Kernphysik, Technische Universität Darmstadt, D-64289 Darmstadt, Germany*

³*Department of Chemistry, Simon Fraser University, Burnaby, British Columbia, V5A 1S6, Canada*

⁴*National Superconducting Cyclotron Laboratory, Michigan State University, East Lansing, Michigan 48824, USA*

⁵*Department of Physics and Astronomy, Michigan State University, East Lansing, Michigan 48824, USA*

⁶*Department of Physics and Astronomy, University of Tennessee, Knoxville, Tennessee 37996, USA*

⁷*Department of Chemistry, Michigan State University, East Lansing, Michigan 48824, USA*

⁸*Saha Institute of Nuclear Physics, Kolkata 700064, India*

⁹*Instituto Nazionale di Fisica Nucleare, Laboratori Nazionali di Legnaro, I-35020 Legnaro, Italy*

¹⁰*Institut für Kernphysik der Universität zu Köln, D-50937 Köln, Germany*

¹¹*Lawrence Livermore National Laboratory, Livermore, California 94551, USA*

¹²*iThemba LABS, PO Box 722, Somerset West 7129, South Africa*

¹³*Department of Fundamental Physics, Chalmers University of Technology, SE-412 96 Göteborg, Sweden*

¹⁴*TRIUMF, 4004 Wesbrook Mall, Vancouver, British Columbia, V6T 2A3, Canada*

Excited states in ^{16}C were populated via the $^9\text{Be}(^{17}\text{N}, ^{16}\text{C}+\gamma)\text{X}$ one-proton knockout reaction. The lifetime of the 2_1^+ state in ^{16}C was measured using the recoil distance method. The extracted lifetime of $\tau_{2_1^+} = 11.4_{-0.9}^{+0.8}(\text{stat}) \pm 0.7(\text{syst}_{B\rho})_{-1.5}^{+0.0}(\text{syst}_{\text{feeding}})$ ps yields a deduced $B(\text{E}2; 2_1^+ \rightarrow 0_1^+) = 4.21_{-0.26}^{+0.34}(\text{stat})_{-0.24}^{+0.28}(\text{syst}_{B\rho})_{-0.00}^{+0.64}(\text{syst}_{\text{feeding}})$ $e^2\text{fm}^4$ value in good agreement with a previous measurement. The one-proton knockout cross section is used to extract the proton amplitude of the ^{16}C 2_1^+ state, which confirms the neutron dominant character of this state. Gamma-ray branching ratios between the 2_2^+ state and the 2_1^+ and ground states were also determined. The results are compared with p - sd Shell Model and No-Core Shell Model (with NN and $NN+NNN$) calculations. The inclusion of three-body forces are essential in order for the No-Core Shell Model calculations to reproduce the experimental findings on the γ -ray branching ratios.

PACS numbers: 27.20.+n, 21.10.Tg, 23.20.Lv

I. INTRODUCTION

The neutron-rich carbon isotopes, which are experimentally accessible up to the neutron dripline, provide the opportunity to study the evolution of nuclear structure as one approaches the dripline. The even-mass neutron-rich carbon isotopes have been extensively studied recently [1–7] since quenched $B(\text{E}2; 2_1^+ \rightarrow 0_1^+)$ values and large asymmetries in the proton (M_p) and neutron (M_n) quadrupole matrix elements, M_n/M_p , were reported and interpreted as evidence of the decoupling of the valence neutrons from the core. In particular, ^{16}C was the first carbon isotope where such an interpretation was applied. A very quenched $B(\text{E}2; 2_1^+ \rightarrow 0_1^+) = 0.63 e^2\text{fm}^4$ was implied from the lifetime measurement of the 2_1^+ state in ^{16}C [1]. This result combined with the deduced M_n and M_p values (from inelastic scattering of a ^{16}C beam on a ^{208}Pb target [2]) suggested a dramatic change in the nuclear structure of ^{16}C compared to the other even-even nuclei in its vicinity. Subsequent work

[3] yielded a nuclear deformation parameter more in line with what is expected from the systematics, but when combined with the lifetime of Ref. [1], the result still indicates an anomalously large ratio M_n/M_p for the 2_1^+ state in ^{16}C . In 2008 the value of the lifetime of the 2_1^+ state in ^{16}C was remeasured by Wiedeking *et al.* [4] and Ong *et al.* [5]. The deduced reduced transition matrix element from these last two lifetime measurements were $B(\text{E}2; 2_1^+ \rightarrow 0_1^+) = 4.15(73) e^2\text{fm}^4$ and $B(\text{E}2; 2_1^+ \rightarrow 0_1^+) = 2.6(2) e^2\text{fm}^4$, respectively. These values for the $B(\text{E}2)$ do not support the scenario of an anomalous decoupling of the valence neutrons from the core.

Here, we report on a new lifetime measurement of the 2_1^+ state in ^{16}C using the recoil distance method with fast radioactive beams. With this measurement we confirm the latest reported value for the lifetime of ^{16}C of Ref. [4]. Moreover, relative partial cross sections for the one-proton knockout to ^{16}C are measured in this work and the extracted proton amplitude of the 2_1^+ state in ^{16}C is presented. Gamma-ray branching ratios between the 2_2^+ state and the 2_1^+ and ground states in ^{16}C are also determined. The results are compared with p - sd Shell Model and *ab initio* No-Core Shell Model calculations.

* mpetri@ikp.tu-darmstadt.de

II. EXPERIMENTAL DETAILS

For this lifetime measurement the recoil distance method (RDM) was employed. The experiment was performed at the National Superconducting Cyclotron Laboratory (NSCL) [8]. The RDM, or plunger technique, with intermediate-energy radioactive beams has been recently developed and tested [9, 10] at the NSCL for lifetime measurements of excited states of exotic nuclei. Physics results from such measurements have already been published [7, 11–14]. In such studies a fast beam reacts with the target and the excited nuclei of interest de-excite by γ -ray emission either before or after passing through the degrader, which is placed downstream of the target, thus inducing different Doppler shifts. In the Doppler-corrected γ -ray spectrum, where a single value for the velocity (v/c) of the ions is used, two peaks that correspond to the same transition emerge depending on where the de-excitation took place with respect to the degrader (see Fig. 1 of Ref. [10]). The relative intensity of these two γ -ray peaks as a function of the target/degrader distance is directly related to the lifetime of the state. This method is ideal for measuring nuclear levels of exotic nuclei with lifetimes in the picosecond range.

A primary ^{22}Ne beam was delivered by the Coupled Cyclotron Facility at the NSCL and fragmented on a thick ^9Be production target (3196 mg/cm^2) at an energy of 150 MeV/nucleon . ^{17}N , the secondary beam of interest, was selected and identified on an event-by-event basis through time-of-flight measurements in the A1900 separator [15] with a purity of $\approx 90\%$ and was delivered to the S3 experimental vault where the S800 spectrometer [16] is located. This RDM measurement made use of the Köln/NSCL plunger [17], which was placed at the target position of the S800 spectrometer with a 1 mm (185 mg/cm^2) ^9Be target and a 1 mm (1660 mg/cm^2) ^{181}Ta degrader. The incoming ^{17}N beam impinged on the secondary-reaction ^9Be target of the plunger with an average rate of 5×10^5 pps, an energy of 72 MeV/nucleon and a momentum dispersion of 0.6% . Excited states in ^{16}C were populated via the $^9\text{Be}(^{17}\text{N}, ^{16}\text{C}+\gamma)\text{X}$ one-proton knockout reaction. The plunger was surrounded by the γ -ray spectrometer SeGA [18], which consisted of fifteen 32-fold segmented high-purity germanium detectors and was coupled to the new digital data acquisition system DDAS [19]. SeGA was configured in two rings with seven detectors at 30° (30.2 cm from the target position) (Ring 1) and eight detectors at 140° (23.3 cm from the target position) (Ring 2) with respect to the beam direction; the angles were chosen to maximize the Doppler shifts of the γ rays emitted in flight from a source moving with velocity $v/c \sim 0.2 - 0.3$ [10]. The segmentation of the detectors allowed for an event-by-event Doppler correction to the γ -ray spectrum. This correction was necessary due to the Doppler-shifted γ rays emitted from the fast moving nuclei ($v/c \sim 36\%$). The γ -ray emission angle was defined from the segment with the largest energy deposition [18, 20]. The reaction products were separated by

the S800 spectrometer and ^{16}C was unambiguously identified on an event-by-event basis through time-of-flight and energy-loss measurements. A figure of the plunger-SeGA setup at the target position of the S800 spectrometer can be seen in Fig. 19 of Ref. [21].

Data were collected for four different target/degrader distances at $100, 400, 900$ and $1650\ \mu\text{m}$ with irradiation times $\sim 6, \sim 5, \sim 9$ and ~ 6 hours, respectively. A run with a target/degrader separation of $20000\ \mu\text{m}$ was used to determine the ratio of the target to degrader reactions (discussed later). Data were also collected using a run with the target only, i.e. the plunger degrader was removed, in order to perform the cross-section measurements.

III. RESULTS

Four γ -ray transitions were identified in coincidence with the ^{16}C fragments, see Fig. 1. Their energies are $1762(2), 2217(2), 2317(5)$ and $2374(3)\text{ keV}$ and the relative intensities of the γ -ray peaks are $100\%, 24\%, 5\%$ and 12% , respectively; the relative intensities of the γ rays include efficiency corrections. These transition energies agree well with the literature [22]. From previous studies the $2217, 2317$ and 2374 keV transitions feed the 2_1^+ state and their spin and parities are assigned as $2_2^+, 3^{(+)}$ and 4^+ , respectively.

In this Section we present results on the quadrupole transition strength of the $2_1^+ \rightarrow 0_1^+$ transition, extracted via the lifetime measurement of the 2_1^+ state. For the higher-lying states, it was not possible to make a direct lifetime measurement. However, limits on the branching ratios of the $2_2^+ \rightarrow 0_1^+$ and $2_2^+ \rightarrow 2_1^+$ transitions are extracted. Finally, we present results on the cross section for populating the ^{16}C 2_1^+ state relative to the 0_1^+ state via the one-proton knockout reaction.

A. Lifetime of the 2_1^+ State and $B(E2; 2_1^+ \rightarrow 0_1^+)$ Transition Strength

For the analysis of the experimental data the use of Monte Carlo simulations is important in order to take into account all the information contained in the data. Such a simulation tool, built upon GEANT4 [23] and ROOT [24] toolkits, has been specifically developed for RDM measurements with fast beams at the NSCL [10] and was used for the analysis of the present experiment. All the experimental conditions that have a measurable effect on the γ -ray peaks are included in the simulation. More specifically, the properties of the incoming ^{17}N beam have been determined using this simulation tool and experimental data as described in Ref. [10]. The thicknesses of the target and degrader were verified, the response function of SeGA was deduced using γ -ray sources and the reaction kinematics were modeled using experimental data. The GEANT4 code was used

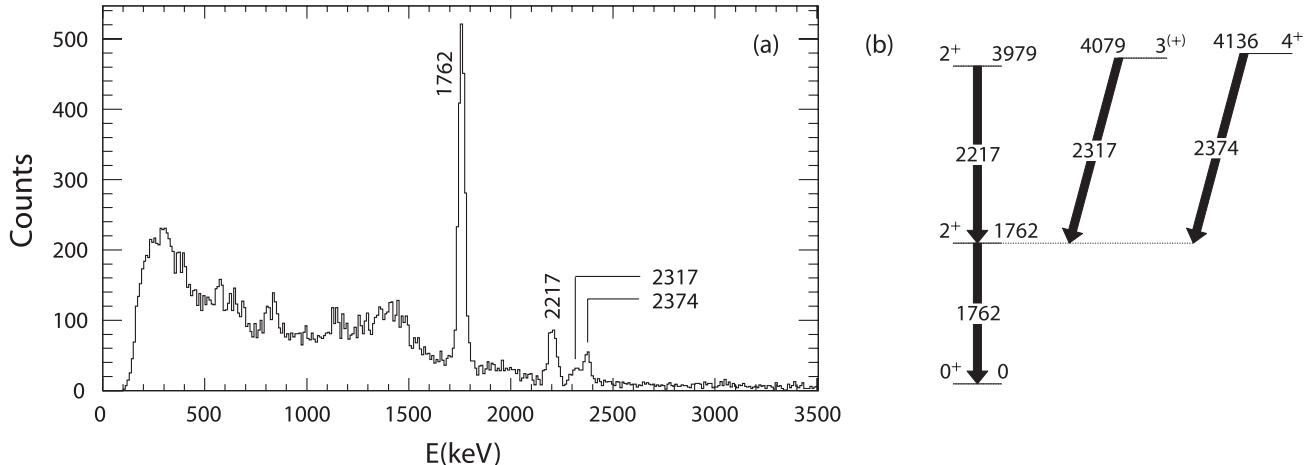


FIG. 1. (a) Gamma-ray spectrum from the backward ring (Ring 2 at 140°) of SeGA from the run with the target only mounted on the plunger device. The observed γ rays are 1762(2), 2217(2), 2317(5) and 2374(3) keV. Their relative intensities are 100%, 24%, 5% and 12%, respectively. (b) Level scheme of ^{16}C as observed in the present experiment.

to model the transport and interaction of heavy ions and γ rays in matter. Background events not included in the Monte Carlo GEANT4 simulation were modeled by adding a linear function to the Monte Carlo spectrum (MC); a local linear background was chosen such that it reproduced the observed background over the energy range of 1200 to 2000 keV. A global exponential background was also used and gave similar results, indicating that the linear background, in a narrow energy region, is a realistic approximation. The final simulated histogram $H_o = aE_\gamma + b + n \cdot MC$, where a and b are background parameters and n is a normalization parameter, is compared to the experimental histogram by performing a point estimation with three free parameters (a, b, n) using the Poisson likelihood chi-square, $\chi_{\lambda,p}^2$, of Ref. [25]. The point estimation was performed from 1200 to 2000 keV, which includes the two peak components and part of the Compton edge. The parameters a, b, n are determined for lifetimes from 7 to 16 ps with a step of 1 ps, i.e. for each lifetime there is a unique “simulated” histogram H_o which is compared to the experimental one. The compatibility of H_o to the experimental spectrum depends now solely on the lifetime of the state. This compatibility is determined via a goodness-of-fit test (using again $\chi_{\lambda,p}^2$ of Ref. [25]) between the “simulated” H_o (expected) histogram and the data (observed) for various lifetimes in an energy region that includes the Doppler-shifted peaks of interest (from 1640 to 1830 keV for Ring 1 and from 1700 to 1920 keV for Ring 2). The simulated and experimental spectra for the lifetime that gives the minimum in the goodness-of-fit test for each target/degrader distance is shown in Fig. 2. We also investigated the dependence of this minimum to the choice of the energy region where the goodness-of-fit is applied and the minimum was found to be rather insensitive.

TABLE I. Lifetime of the 2_1^+ state in ^{16}C from the minimization of each target/degrader distance in each ring (at 30° and 140°).

	100 μm	400 μm	900 μm	1650 μm
Ring 1 (30°)	11.3(10) ps	11.0(9) ps	11.1(7) ps	12.4(9) ps
Ring 2 (140°)	11.1(8) ps	11.0(10) ps	12.6(8) ps	10.5(12) ps

The lifetime for which the $\chi_{\lambda,p}^2$ is minimized, following the aforementioned procedure for each ring and each target/degrader distance, is shown in Table I. The resulting, total $\chi_{\lambda,p}^2$ in both Rings 1 and 2 and for all distances is shown in Fig. 3 for simulated lifetimes between 7 and 16 ps. The lifetime of the 2_1^+ state in ^{16}C is deduced to be $\tau_{2_1^+} = 11.4 \pm 0.3(\text{stat})$ ps from the $\chi_{\lambda,p}^2$ minimization, in very good agreement with the previous measurement of Ref. [4].

There are two dominant sources of uncertainty in this measurement: the uncertainty in the ratio of the number of reactions on the target and degrader, and the uncertainty (up to 0.5%) of the $B\rho$ setting of the spectrometer, i.e. an uncertainty in the simulated momentum distribution of the ^{16}C fragments. Both sources of error have been investigated in detail and are discussed in the next two paragraphs.

In RDM measurements with fast beams the unreacted beam that emerges from the target is energetic enough to generate reactions on the degrader, i.e. in this experiment ^{16}C can be produced via the reactions $^9\text{Be}(^{17}\text{N}, ^{16}\text{C}+\gamma)\text{X}$ and $^{181}\text{Ta}(^{17}\text{N}, ^{16}\text{C}+\gamma)\text{X}$. These products are not well separated in the S800 spectrometer; this one-proton knockout reaction leads to the overlap of the low momentum tail of the fragments produced in

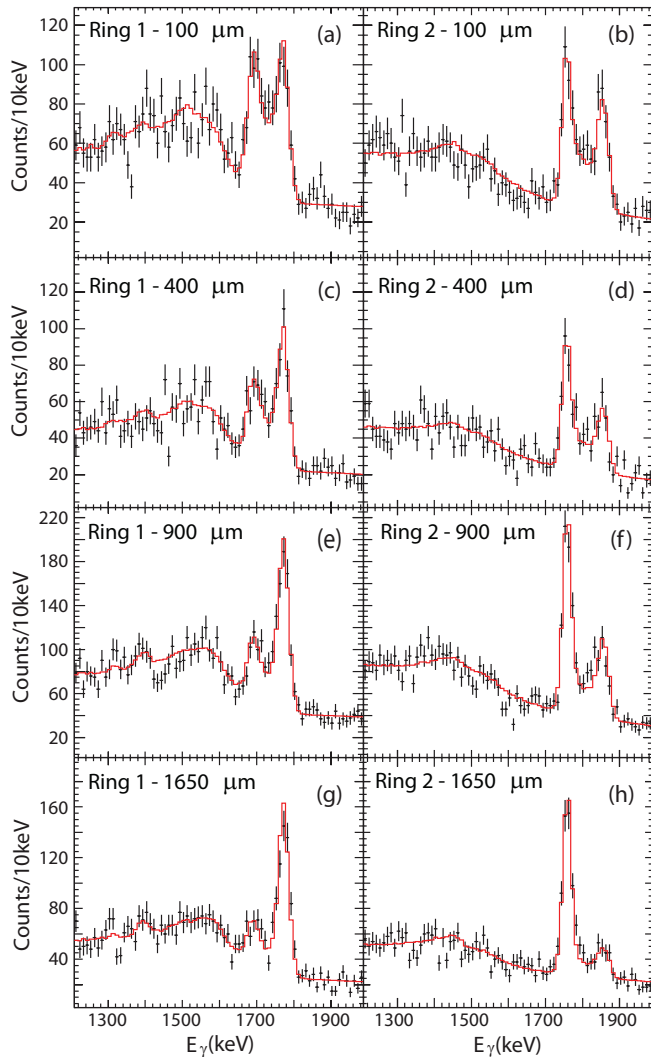


FIG. 2. (Color online) Experimental data (black points with error bars) and the “simulated” histogram H_o (red solid line) (discussed in the text) for the lifetime that minimizes the goodness-of-fit test for the 1762 keV $2_1^+ \rightarrow 0_1^+$ transition in ^{16}C . Spectra (a), (c), (e) and (g) show the experimental data and simulation for Ring 1 (the forward ring at 30°) for target/degrader separation distances of 100, 400, 900 and 1650 μm , respectively. Spectra (b), (d), (f) and (h) show the experimental data and simulation for Ring 2 (the backward ring at 140°) for target/degrader separation distances of 100, 400, 900 and 1650 μm , respectively. The linear background has been fitted for the energy range 1200 to 2000 keV for both rings. The goodness-of-fit has been applied in the energy region of 1640–1830 keV for Ring 1 and 1700–1920 keV for Ring 2.

the target with the high momentum tail of the fragments produced in the degrader. Therefore knowledge of the ratio of the number of reactions on the target and degrader, which is included in the simulation, is important for an accurate extraction of the lifetime. This ratio was derived experimentally, as opposed to using

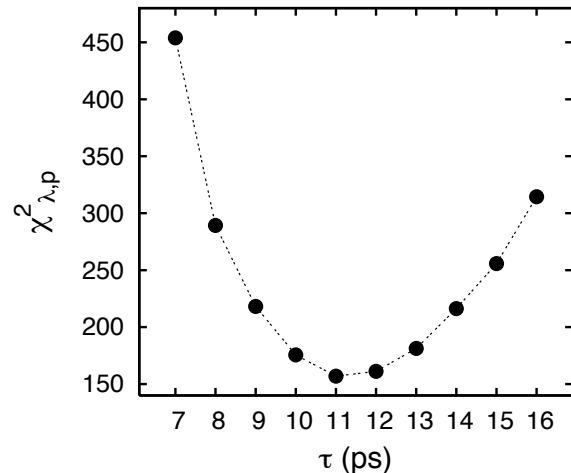


FIG. 3. The lifetime of the $2_1^+ \rightarrow 0_1^+$ transition in ^{16}C is deduced at $\tau_{2_1^+} = 11.4 \pm 0.3$ (statistical) from the minimization in the (total) $\chi^2_{\lambda,p}$. The number of degrees of freedom for this fit is 156.

action cross-section considerations, by setting the separation of the target and degrader in the plunger to be 20000 μm , which corresponds to ~ 20 lifetimes of the 2_1^+ state of ^{16}C . This means that the ratio of the fast and slow component depends solely on the ratio of the number of reactions induced by the target and degrader, respectively. The ratio of the number of reactions on the target over the number of reactions on the degrader deduced from the 20000 μm target/degrader distance run was $1.8^{+0.5}_{-0.4}$. This value was used in the simulation and its error determined the uncertainty in the lifetime induced from this factor to be $^{+0.7}_{-0.8}$ ps. This error is combined in quadrature with the error induced from the minimization procedure (0.3 ps) to yield the total statistical error in this lifetime measurement, $\tau_{2_1^+} = 11.4^{+0.8}_{-0.9}(\text{stat})$ ps. This lifetime yields an electric quadrupole transition rate of $B(E2; 2_1^+ \rightarrow 0_1^+) = 4.21^{+0.34}_{-0.26}(\text{stat}) e^2\text{fm}^4$ for ^{16}C , which is shown in Fig. 4 together with the previous reported values [4, 5]. The current B(E2) confirms the value of Ref. [4].

The error induced from the uncertainty in the $B\rho$ setting of the spectrometer was treated by generating simulations with a 0.5% change in the momentum distribution of the ^{16}C fragments (towards low and high momenta). The full analysis is then repeated for these extreme $\pm 0.5\%$ $B\rho$ settings and the error in the lifetime due to this uncertainty was determined at ± 0.7 ps. This error is treated as a systematic one and is denoted as $\text{syst}_{B\rho}$.

Taking into account all aforementioned uncertainties, the lifetime of the 2_1^+ state in ^{16}C is $\tau_{2_1^+} = 11.4^{+0.8}_{-0.9}(\text{stat}) \pm 0.7(\text{syst}_{B\rho})$ ps. This lifetime yields a deduced $B(E2; 2_1^+ \rightarrow 0_1^+) =$

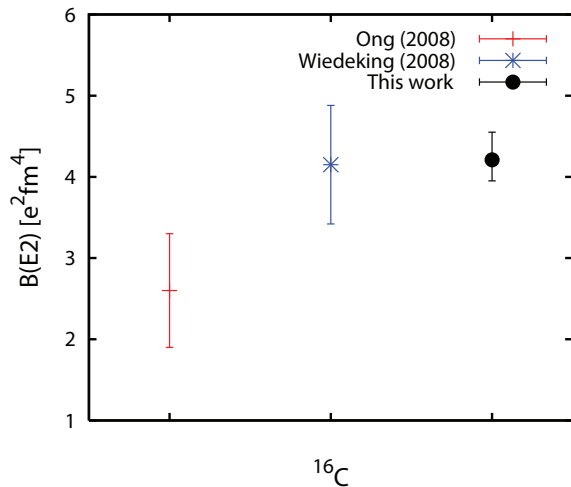


FIG. 4. (Color online) $B(E2; 2_1^+ \rightarrow 0_1^+)$ values for ^{16}C as reported in Ref. [4] (Wiedeking (2008)), Ref. [5] (Ong(2008)) and in this work. The $B(E2)$ values are shown with their statistical errors only.

$$4.21^{+0.34}_{-0.26}(\text{stat})^{+0.28}_{-0.24}(\text{syst}_{B\rho}) e^2\text{fm}^4.$$

B. Transitions from Higher-Lying States

Three additional higher-lying states were observed, the 2_2^+ , the 4^+ and the $3^{(+)}$, which feed the 2_1^+ state. The $2_2^+ \rightarrow 2_1^+$ transition proceeds very rapidly; no obvious slow component is observed from its de-excitation after passing through the degrader in the 100 μm target/degrader separation distance data. This observation leads to an upper limit for the lifetime of roughly 4 ps, in agreement with previous observations [4]. A Doppler Shift Attenuation Method measurement (appropriate for short lifetimes) cannot be performed with the current thickness of the target to determine the lifetime of the 2_2^+ state. The $3_1^{(+)} \rightarrow 2_1^+$ and $4_1^+ \rightarrow 2_1^+$ transitions are not observed in the plunger data due to limited statistics. Therefore no conclusion with respect to their lifetime can be drawn from this experiment. A previous measurement [4], however, has determined these two transitions to be faster than the $2_1^+ \rightarrow 0_1^+$ transition with their lifetimes being shorter than 4 ps. The maximal error that is induced in our measurement from the lifetime of the feeding transitions can be estimated if we assume that all three transitions have the longest possible lifetime of 4 ps. Then the lifetime of the $2_1^+ \rightarrow 0_1^+$ transition is estimated to be 1.5 ps shorter than the one measured. The systematic error therefore due to the feeding transitions is $^{+0.0}_{-1.5}(\text{syst}_{\text{feeding}})$ ps. The lifetime of the 2_1^+ state in ^{16}C is then $\tau_{2_1^+} = 11.4^{+0.8}_{-0.9}(\text{stat}) \pm 0.7(\text{syst}_{B\rho})^{+0.0}_{-1.5}(\text{syst}_{\text{feeding}})$ ps and $B(E2; 2_1^+ \rightarrow 0_1^+) = 4.21^{+0.34}_{-0.26}(\text{stat})^{+0.28}_{-0.24}(\text{syst}_{B\rho})^{+0.64}_{-0.00}(\text{syst}_{\text{feeding}}) e^2\text{fm}^4$.

In the experimental spectrum no transition from the 2_2^+ state to the ground state was observed. This sets

a limit on the branching ratios for the $2_2^+ \rightarrow 2_1^+$ and $2_2^+ \rightarrow 0_1^+$ transitions. These limits were set based on the number of counts observed for the $2_2^+ \rightarrow 2_1^+$ transition and the standard deviation σ , which takes into account the background fluctuations in the energy regime where the $2_2^+ \rightarrow 0_1^+$ transition is expected. No peak is observed in the region where the $2_2^+ \rightarrow 0_1^+$ transition is expected and based on background statistics we obtain limits on the branching ratio for the $2_2^+ \rightarrow 2_1^+$ transition $\text{BR}(2_2^+ \rightarrow 2_1^+) > 91.2\%$ and for the $2_2^+ \rightarrow 0_1^+$ transition $\text{BR}(2_2^+ \rightarrow 0_1^+) < 8.8\%$, at the 3σ confidence level.

C. Relative Partial Cross Section

Data were collected using the target only, i.e. the degrader was removed from the plunger, allowing therefore, relative partial cross sections to be measured in this one-proton knockout reaction. For this cross-section measurement only detectors in Ring 2 (140°) were used. The reason for this choice is that the γ -ray energies in the laboratory frame detected by the backward (Ring 2) detectors are shifted to lower energies due to the Doppler effect. In this energy region the energy resolution is better and the energy and efficiency measurements more reliable, since they are closer to the region covered by a ^{152}Eu calibration source. The expected alignment in this one-proton knockout is very small [26] and therefore no correction for the γ -ray angular distribution is considered when using only the backward detectors. The cross section for populating the 2_1^+ state in ^{16}C over its ground state has been measured to be $\sigma(2_1^+)/\sigma(0_1^+) = 0.28 \pm 0.02$.

IV. DISCUSSION

We now compare the measured $B(E2; 2_1^+ \rightarrow 0_1^+)$ values and excited-state branching ratios (which also depend on transition strengths), as well as results from reaction cross-section data to those from $p - sd$ Shell Model and *ab initio* No-Core Shell Model (NCSM) [27] calculations.

The $p - sd$ Shell Model calculations were performed using the OXBASH shell model code [28] with three different sets of empirically derived two-body nucleon-nucleon effective interactions referred to as WBP [29], WBT [29] and WBT* [30]. These calculations use harmonic oscillator wavefunctions and are carried out in the p shell model space for protons and the sd shell model space for neutrons. Neutron holes in the p shell have been ignored. The reason is that the excitation of neutrons from p to sd are Pauli blocked by the neutrons that occupy sd . The variants of WBP and WBT Hamiltonians can be used to gauge the theoretical error within the context of the $p - sd$ model space. In the WBT* interaction the neutron-neutron two-body matrix elements are reduced to 75% of those in WBT. This was introduced in Ref. [30] to describe the fact that the experimental excitation spectra for carbon isotopes are systematically

compressed compared to the calculations carried out with WBT. A discussion of the neutron-rich carbon isotopes ($^{16,18,20}\text{C}$) within a p - sd Shell Model is given in Ref. [7].

The large-scale *ab initio* NCSM calculations used three different NN interactions: the CDB2k [31] based on one-boson exchange theory, the INOY [32] that introduces a nonlocality to simulate some effects of three-nucleon forces, and the chiral N^3LO NN potential of Ref. [33] derived within chiral perturbation theory. Calculations with the chiral N^3LO NN potential augmented by a local chiral N^2LO NNN potential parametrized according to Ref. [34] were also performed. A detailed description of these NCSM calculations is given in Ref. [35], where the results of calculations for low-lying states of even-even carbon isotopes, including the systematics of 2^+ states, are presented. Here we give a brief summary of these calculations. NCSM calculations were performed using a harmonic-oscillator (HO) basis truncated by a total HO energy cutoff, characterized by the maximal number of HO excitations N_{max} above the unperturbed ground state. To use the largest N_{max} possible we employed the Importance-Truncated No-Core Shell Model (IT-NCSM) scheme [36–38]. Within this scheme, basis states which are not important for the description of the ground state and low-lying states are identified via many-body perturbation theory and excluded from the calculation. Therefore, only the important basis states remain and the dimension of the matrix eigenvalue problem is reduced without losing predictive power. In addition, due to the strong short-range correlations generated by the NN potentials, effective interactions are used to speed up convergence, which were derived by performing unitary transformations in the two-nucleon HO basis. The results exhibit a dependence on N_{max} and the HO frequency $\hbar\Omega$ that should disappear once complete convergence is reached, that is N_{max} sequences obtained with different $\hbar\Omega$ should all converge to the same result. However, full convergence of spectroscopic observables with respect to N_{max} cannot be reached for the heavy carbon isotopes discussed here. Therefore calculations are performed for a series of finite N_{max} values at varying $\hbar\Omega$ and a constrained fit is then applied to these multiple sequences in order to extrapolate to the infinite, un-truncated model space result [35, 39]. Examples of these extrapolation procedures for carbon isotopes are shown in Fig. 2 of Ref. [35].

A. $\text{B}(\text{E}2; 2_1^+ \rightarrow 0_1^+)$ Transition Strength

Table II compares the experimental $\text{B}(\text{E}2; 2_1^+ \rightarrow 0_1^+)$ value with those from p - sd Shell Model and *ab initio* No-Core Shell Model (NCSM) [27] calculations.

Within the p - sd Shell Model the electric quadrupole transition rate is derived from the equation

$$\text{B}(\text{E}2; J_i \rightarrow J_f) = |M_p e_p + M_n e_n|^2 / (2J_i + 1),$$

where M_p and M_n are shell model proton and neutron quadrupole matrix elements connecting the J_i and J_f states (in this case the $J_i = 2_1^+$ and $J_f = 0_1^+$ states). Here, the matrix elements were calculated using the WBP, WBT and WBT* interactions. The effective charges, $e_p = 1.16$ and $e_n = 0.33$, are taken from the calculation in Ref. [40] and follow an approximate $1/A$ dependence based on the treatment in Ref. [41]. The results of these calculations agree well with the current experimental value of $4.21 e^2\text{fm}^4$.

The $\text{B}(\text{E}2; 2_1^+ \rightarrow 0_1^+)$ value obtained with the NCSM calculation using the CDB2k interaction is also presented. In this case the calculation does not assume an inert core and effective charges are not used. It is seen that this NN interaction predicts a lower $\text{B}(\text{E}2; 2_1^+ \rightarrow 0_1^+)$ value than either the p - sd Shell Model or the latest data, by about a factor of two. We note that, as discussed in Ref. [35], the convergence behavior for the $\text{B}(\text{E}2)$ in ^{16}C is different from that seen in the neighboring carbon isotopes, where the calculated $\text{B}(\text{E}2)$ s show better agreement with data. For the INOY interaction the specific model-space and frequency dependence of the $\text{B}(\text{E}2)$ does not allow for a reliable extrapolation, therefore, no value is reported here. Finally, to study the effects of higher order interactions we performed calculations using the chiral NN interaction and chiral $NN + NNN$. Calculations with NNN terms in the Hamiltonian are computationally more intense and in particular the extrapolation to obtain an absolute $\text{B}(\text{E}2)$ value is difficult. Preliminary results indicate that the $\text{B}(\text{E}2)$ obtained with the chiral NN interaction is close to that of CDB2k, while chiral $NN + NNN$ yields smaller $\text{B}(\text{E}2)$ values. While Ref. [35] shows that NCSM (NN) calculations give an overall good description of the $\text{B}(\text{E}2; 2_1^+ \rightarrow 0_1^+)$ for even-even carbon isotopes ($^{10-20}\text{C}$), the value for ^{16}C is underestimated. Future investigations will show to what extent this observable is sensitive to the chiral $\text{NN}+3\text{N}$ Hamiltonian, particularly to the inclusion of consistent 3N interactions at order N^3LO or to the variation of cutoffs and low-energy constants.

B. Energies and Branching Ratios of Higher-Lying States

In Fig. 5 calculated energy levels of ^{16}C are shown and compared with experiment. As mentioned before, within the p - sd Shell Model there is a better agreement between calculated and experimental values when using the WBT* interaction. For the NCSM, the agreement with experiment is quite reasonable when using the chiral N^3LO NN potential (with and without the NNN interaction), although improved in the calculation with the chiral $NN + NNN$ Hamiltonian.

In Section III B it was shown that the second 2^+ state at 3979 keV decays primarily to the first 2^+ state at 1762 keV, with only a weak ($< 8.8\%$) branch to the ground state. This branching ratio depends on the $\text{B}(\text{E}2;$

TABLE II. Experimental value and predictions from the $p - sd$ Shell Model using three interactions, the WBP, WBT and WBT*, and extrapolated *ab initio* NCSM results obtained with the CDB2k NN interaction for the ^{16}C $B(E2; 2_1^+ \rightarrow 0_1^+)$.

	Experiment	WBP	WBT	WBT*	CDB2k	Unit
$B(E2; 2_1^+ \rightarrow 0_1^+)$	$4.21_{-0.26}^{+0.34}(\text{stat})_{-0.24}^{+0.28}(\text{sys}_{B\rho})_{-0.00}^{+0.64}(\text{sys}_{\text{feeding}})$	4.672	4.208	3.943	2.2 ± 0.6	$e^2\text{fm}^4$

$2_2^+ \rightarrow 2_1^+$), $B(E2; 2_2^+ \rightarrow 0_1^+)$ and $B(M1; 2_2^+ \rightarrow 2_1^+)$ values and can be used to further test theory. Table III contains the calculated branching ratios for the $2_2^+ \rightarrow 2_1^+$ and $2_2^+ \rightarrow 0_1^+$ transitions for various $p - sd$ Shell Model and NCSM interactions. The values from the $p - sd$ Shell Model agree with observation. However, NN interactions (CDB2k, chiral NN) used in the NCSM calculation show the opposite, whereby the $2_2^+ \rightarrow 0_1^+$ transition dominates and carries more than 67.6% of the decay. If this were the case then we would have observed in our data more than 556 counts in the $2_2^+ \rightarrow 0_1^+$ transition (a 65σ peak). Including NNN interactions (chiral $NN + NNN$) has a big effect and leads to a branching ratio that is consistent with experiment. We note that while the absolute $B(E2)$ values depend critically on the convergence, the branching ratios $2_2^+ \rightarrow 2_1^+$ and $2_2^+ \rightarrow 0_1^+$, which depend on the relative E2 strengths and $B(M1; 2_2^+ \rightarrow 2_1^+)$ value, are not sensitive to the absolute values of the $B(E2)$, i.e. changing the $B(E2)$ values by a factor of 2 will not change the branching ratios significantly. It is found that including NNN interactions significantly increases the $B(M1)$. The sensitivity of the branching ratio to the inclusion of NNN terms suggests such data on excited state properties can be important and used to guide *ab initio* theories.

C. Proton Amplitude of the 2_1^+ State

In a simple shell model picture the ground state wave function of ^{17}N can be written as

$$|1/2^-; ^{17}\text{N}\rangle = |\nu(sd)^2; J = 0\rangle \otimes |\pi(p)^{-1}; J = 1/2\rangle$$

and the 2_1^+ and 0^+ ground state of ^{16}C :

$$|2_1^+; ^{16}\text{C}\rangle = \alpha|\nu(sd)^2; J = 2\rangle \otimes |\pi(p)^{-2}; J = 0\rangle + \beta|\nu(sd)^2; J = 0\rangle \otimes |\pi(p)^{-2}; J = 2\rangle,$$

$$|0^+; ^{16}\text{C}\rangle = \gamma|\nu(sd)^2; J = 0\rangle \otimes |\pi(p)^{-2}; J = 0\rangle + \delta|\nu(sd)^2; J = 2\rangle \otimes |\pi(p)^{-2}; J = 2\rangle.$$

Because of the expected higher excitation energy of the $|\nu(sd)^2; J = 2\rangle \otimes |\pi(p)^{-2}; J = 2\rangle$ component of the 0^+ in ^{16}C , we can assume $\delta \approx 0$, $\gamma = 1$ and

$$|0^+; ^{16}\text{C}\rangle = |\nu(sd)^2; J = 0\rangle \otimes |\pi(p)^{-2}; J = 0\rangle.$$

Therefore the measurement of the cross section for populating the 2_1^+ over the ground state can provide the proton amplitude of the 2_1^+ state. By knocking-out one proton from the $p_{1/2}$ shell we can only go to the ground

state of ^{16}C , while by knocking-out one proton from the $p_{3/2}$ shell we can go to either a 2^+ or a 1^+ state. The probability for populating the 2^+ state by knocking-out one of the four $p_{3/2}$ protons is then $4 \times 5/8$ and the probability for populating the 0^+ by knocking-out the only $p_{1/2}$ proton is 1. The population of the 2_1^+ state in ^{16}C via the one-proton knockout reaction $^9\text{Be}(^{17}\text{N}, ^{16}\text{C} + \gamma)\text{X}$ proceeds through the proton component (the neutron 2^+ cannot couple to the ground state of ^{17}N) and therefore, the ratio of the spectroscopic factors $C^2S(2_1^+)/C^2S(0_1^+)$ is approximately equal to $(\beta^2 \times 5/2)/1$, according to the aforementioned sum rules.

From reaction theory [42] the cross sections for populating the 2_1^+ and 0^+ states are

$$\sigma(2_1^+) = C^2S(2_1^+)\sigma_{th}^{2_1^+}, \sigma(0^+) = C^2S(0^+)\sigma_{th}^{0^+}.$$

Since the ℓ of the knocked-out proton is the same in both cases ($\ell = 1$) and the levels are strongly bound, we assume that $\sigma_{th}^{2_1^+} \approx \sigma_{th}^{0^+}$. The ratio of the cross sections for populating the 2_1^+ and ground states in ^{16}C , $\sigma(2_1^+)/\sigma(0_1^+)$, is then approximately equal to the ratio of the spectroscopic factors $C^2S(2_1^+)/C^2S(0_1^+)$, i.e.

$$\sigma(2_1^+)/\sigma(0_1^+) \approx C^2S(2_1^+)/C^2S(0_1^+) \approx \beta^2 \times 5/2.$$

This ratio has been measured experimentally to be 0.28 ± 0.02 (see Section III C) and thus the proton amplitude in the ^{16}C 2_1^+ state is $\beta^2 \approx 11(1)\%$.

A comparison between the experimentally determined proton amplitude of the 2_1^+ state in ^{16}C and the theoretical estimates from the $p - sd$ Shell Model and the NCSM is shown in Table IV. The $p - sd$ Shell Model calculations underestimate β^2 . The NCSM using the CDB2k and the chiral NN interactions estimates a proton amplitude for the 2_1^+ state of ^{16}C in line with the experimentally determined value, whereas the chiral $NN + NNN$ interaction falls between the $p - sd$ Shell Model and the experimental value.

The experimentally determined proton amplitude of the 2_1^+ state in ^{16}C confirms the neutron dominant character of this state, in agreement with other measurements [43]. This finding is also confirmed by studying the occupation numbers of the NCSM wave functions, see Ref. [35]. It will be interesting to measure the proton amplitude in the heavier carbon isotopes $^{18,20}\text{C}$ in order to confirm the increase in the proton contribution to their 2_1^+ state as suggested by the latest ^{20}C lifetime measurement [7].

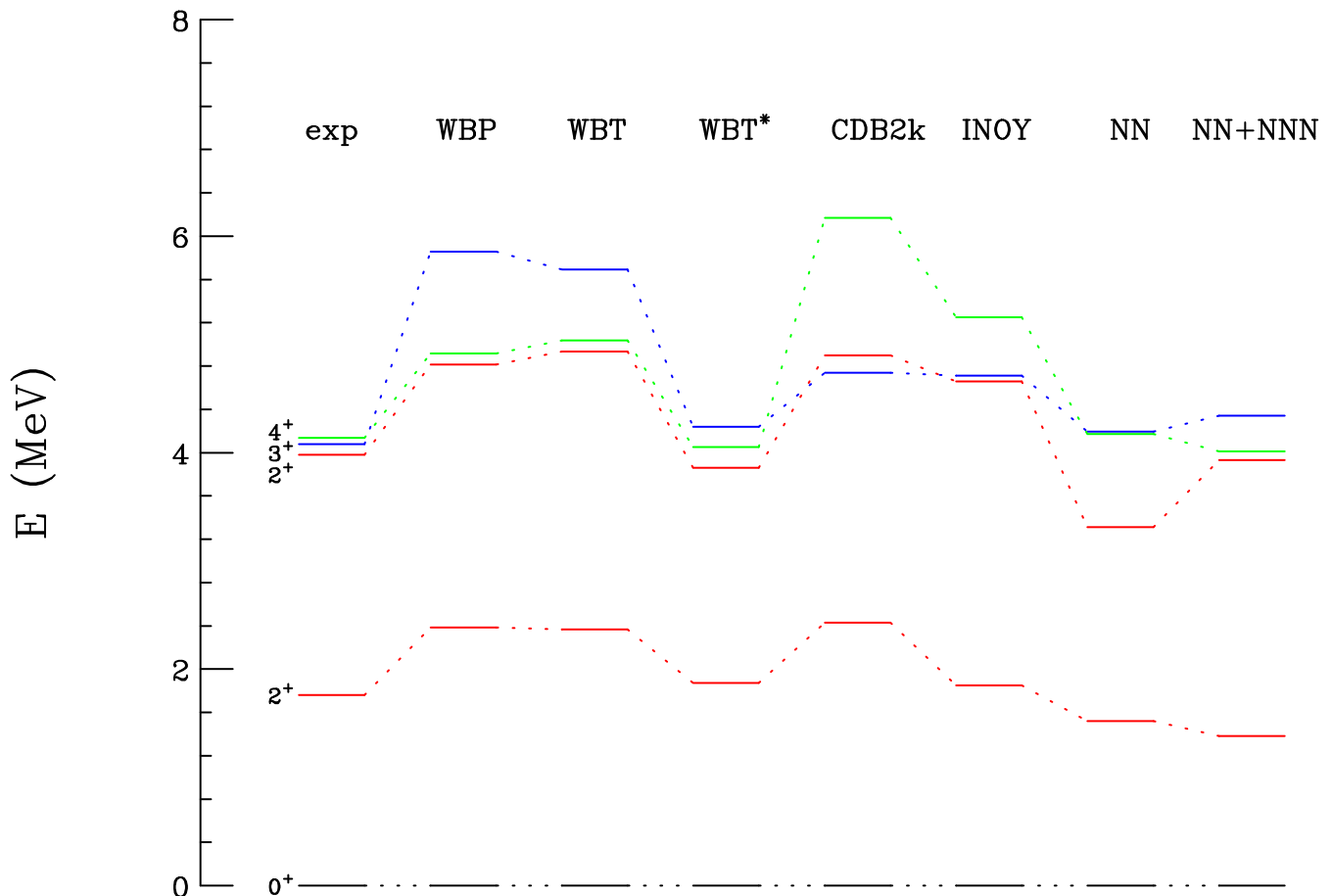


FIG. 5. (Color online) Excitation energies of the lowest states of ^{16}C . Calculated levels with the $p-sd$ Shell Model using WBP, WBT and WBT* interactions and with the NCSM using the CDB2k, INOY, chiral NN and chiral $NN + NNN$ potential are compared with the experimentally determined values (exp).

TABLE III. Branching ratios for the $2_2^+ \rightarrow 2_1^+$ and $2_2^+ \rightarrow 0_1^+$ transitions obtained from experiment, the NCSM calculations with the CDB2k and the chiral NN potential with and without the chiral NNN interaction, and the $p-sd$ Shell Model calculations with the WBP, WBT and WBT* interactions. The experimental data sets a limit for these ratios based on the non-observation of the $2_2^+ \rightarrow 0_1^+$ transition.

	Experiment	CDB2k	NN	$NN + NNN$	WBP	WBT	WBT*
$2_2^+ \rightarrow 2_1^+$	$> 91.2\%$	32.4%	21.6%	97.6%	92.2%	93.2%	97.6%
$2_2^+ \rightarrow 0_1^+$	$< 8.8\%$	67.6%	78.4%	2.4%	7.8%	6.8%	2.4%

V. CONCLUSION

The lifetime of the 2_1^+ state in ^{16}C has been measured using the recoil distance method with fast radioactive ion beams. The extracted lifetime of $\tau_{2_1^+} = 11.4_{-0.9}^{+0.8}(\text{stat}) \pm 0.7(\text{syst}_{B\rho})_{-1.5}^{+0.0}(\text{syst}_{\text{feeding}})$ ps is in very good agreement with the previous measurement of Ref. [4]. The deduced $B(E2; 2_1^+ \rightarrow 0_1^+) = 4.21_{-0.26}^{+0.34}(\text{stat})_{-0.24}^{+0.28}(\text{syst}_{B\rho})_{-0.00}^{+0.64}(\text{syst}_{\text{feeding}})$ $e^2\text{fm}^4$ is compared with theoretical predictions using the $p-sd$ Shell Model and the No-Core Shell Model. The $p-sd$ Shell Model reproduces the experimentally deduced

$B(E2)$ value well. The NCSM, with microscopic wave functions and bare nucleon charges, underestimate this value in the model spaces that were reached in this study. The rather slow convergence of this observable is probably connected with the particular neutron-excitation structure of the 2_1^+ state, see Ref. [35]. Gamma-ray branching ratios from higher-lying transitions seem to indicate the need to include three-body forces in order for the NCSM to reproduce the experimental results. The small proton amplitude of the 2_1^+ state in ^{16}C ($\beta^2 = 11(1)\%$) verifies the neutron dominant character of this state.

TABLE IV. Spectroscopic factors and proton amplitude of the 2_1^+ state in ^{16}C from experiment, the $p - sd$ Shell Model and the NCSM calculations.

	Experiment	WBP	WBT	WBT*	CDB2k	NN	$NN + NNN$
$C^2S(2_1^+)/C^2S(0_1^+)$	0.28 ± 0.02	0.156	0.104	0.086	0.21	0.33	0.15
proton amplitude (β^2)	11(1)%	6.2%	4.2%	3.4%	8.4%	13.2%	6.0%

ACKNOWLEDGMENTS

The authors acknowledge the help of the NSCL operations staff. M.P. would like to thank H. Iwasaki for fruitful discussions. This work is supported in part by the Director, Office of Science, Office of Nuclear Physics, of the U.S. Department of Energy under contracts No. DE-

AC02-05CH11231 and No. DE-AC52-07NA27344, and by the National Science Foundation under grant PHY-0606007 and PHY-1068217. C.F. acknowledges support from the Swedish Research Council and the European Research Council under the FP7. R.R. acknowledges support from DFG through SFB 634, HIC for FAIR, and the JSC.

-
- [1] N. Imai *et al.*, Phys. Rev. Lett., **92**, 062501 (2004).
[2] Z. Elekes *et al.*, Phys. Lett. B, **586**, 34 (2004).
[3] H. J. Ong *et al.*, Phys. Rev. C, **73**, 024610 (2006).
[4] M. Wiedeking *et al.*, Phys. Rev. Lett., **100**, 152501 (2008).
[5] H. J. Ong *et al.*, Phys. Rev. C, **78**, 014308 (2008).
[6] Z. Elekes *et al.*, Phys. Rev. C, **79**, 011302(R) (2009).
[7] M. Petri *et al.*, Phys. Rev. Lett., **107**, 102501 (2011).
[8] <http://www.nsl.mscl.edu/>.
[9] A. Chester *et al.*, Nucl. Instrum. Methods Phys. Res. Sec. A, **562**, 230 (2006).
[10] P. Adrich *et al.*, Nucl. Instrum. Methods Phys. Res. Sec. A, **598**, 454 (2009).
[11] K. Starosta *et al.*, Phys. Rev. Lett., **99**, 042503 (2007).
[12] A. Dewald *et al.*, Phys. Rev. C, **78**, 051302R (2008).
[13] W. Rother *et al.*, Phys. Rev. Lett., **106**, 022502 (2011).
[14] P. Voss *et al.*, Phys. Rev. C, **86**, 011303 (2012).
[15] D. J. Morrissey *et al.*, Nucl. Instrum. Methods Phys. Res. Sec. B, **204**, 90 (2003).
[16] D. Bazin *et al.*, Nucl. Instrum. Methods Phys. Res. Sec. B, **204**, 629 (2003).
[17] A. Dewald *et al.*, GSI Scientific Report 2005, p. 38 (2006).
[18] W. F. Mueller *et al.*, Nucl. Instrum. Methods Phys. Res. Sec. A, **466**, 492 (2001).
[19] K. Starosta *et al.*, Nucl. Instrum. Methods Phys. Res. Sec. A, **610**, 700 (2009).
[20] A. Gade and T. Glasmacher, Progress in Particle and Nuclear Physics, **60**, 161 (2008), ISSN 0146-6410.
[21] A. Dewald, O. Möller, and P. Petkov, Progress in Particle and Nuclear Physics, **67**, 786 (2012).
[22] D. R. Tilley, H. R. Weller, and C. M. Cheves, Nucl. Phys. A, **564**, 1 (1993).
[23] S. Agostinelli *et al.*, Nucl. Instrum. Methods Phys. Res. Sec. A, **506**, 250 (2003).
[24] R. Brun and F. Rademakers, Nucl. Instrum. Methods Phys. Res. Sec. A, **389**, 81 (1997).
[25] S. Baker and R. D. Cousins, Nucl. Instrum. Methods Phys. Res., **221**, 437 (1984).
[26] J. A. Tostevin, private communication (2012).
[27] P. Navrátil, J. P. Vary, and B. R. Barrett, Phys. Rev. Lett., **84**, 5728 (2000).
[28] B. A. Brown *et al.*, MSU-NSCL Report No. 524.
[29] E. K. Warburton and B. A. Brown, Phys. Rev. C, **46**, 923 (1992).
[30] M. Stanoiu *et al.*, Phys. Rev. C, **78**, 034315 (2008).
[31] R. Machleidt, Phys. Rev. C, **63**, 024001 (2001).
[32] P. Doleschall, Phys. Rev. C, **69**, 054001 (2004).
[33] D. R. Entem and R. Machleidt, Phys. Rev. C, **68**, 041001 (2003).
[34] D. Gazit, S. Quaglioni, and P. Navrátil, Phys. Rev. Lett., **103**, 102502 (2009).
[35] C. Forssén, R. Roth, and P. Navrátil, arXiv:1110.0634v2 [nucl-th] (2011).
[36] R. Roth, J. Langhammer, A. Calci, S. Binder, and P. Navrátil, Phys. Rev. Lett., **107**, 072501 (2011).
[37] R. Roth and P. Navrátil, Phys. Rev. Lett., **99**, 092501 (2007).
[38] R. Roth, Phys. Rev. C, **79**, 064324 (2009).
[39] C. Forssén, J. P. Vary, E. Caurier, and P. Navrátil, Phys. Rev. C, **77**, 024301 (2008).
[40] H. Sagawa, X. R. Zhou, X. Z. Zhang, and T. Suzuki, Phys. Rev. C, **70**, 054316 (2004).
[41] A. Bohr and B. R. Mottelson, *Nuclear Structure*, Vol. 2 (W. A. Benjamin, Massachusetts, 1975) p. 514.
[42] P. Hansen and J. Tostevin, Annual Review of Nuclear and Particle Science, **53**, 219 (2003).
[43] A. H. Wuosmaa *et al.*, Phys. Rev. Lett., **105**, 132501 (2010).